THE JOURNAL OF BIOLOGICAL CHEMISTRY VOL. 284, NO. 18, pp. 12031–12040, May 1, 2009

Domain Architecture of the Stator Complex of the A_1A_0-ATP Synthase from *Thermoplasma acidophilum*[*] [S]

Received for publication, November 26, 2008, and in revised form, February 18, 2009 Published, JBC Papers in Press, February 20, 2009, DOI 10.1074/jbc.M808962200

Erik Kish-Trier and Stephan Wilkens[1]

From the Department of Biochemistry & Molecular Biology, SUNY Upstate Medical University, Syracuse, New York 13210

A key structural element in the ion translocating F-, A-, and V-ATPases is the peripheral stalk, an assembly of two polypeptides that provides a structural link between the ATPase and ion channel domains. Previously, we have characterized the peripheral stalk forming subunits E and H of the A-ATPase from *Thermoplasma acidophilum* and demonstrated that the two polypeptides interact to form a stable heterodimer with 1:1 stoichiometry (Kish-Trier, E., Briere, L. K., Dunn, S. D., and Wilkens, S. (2008) *J. Mol. Biol.* 375, 673–685). To define the domain architecture of the A-ATPase peripheral stalk, we have now generated truncated versions of the E and H subunits and analyzed their ability to bind each other. The data show that the N termini of the subunits form an α-helical coiled-coil, ~80 residues in length, whereas the C-terminal residues interact to form a globular domain containing α- and β-structure. We find that the isolated C-terminal domain of the E subunit exists as a dimer in solution, consistent with a recent crystal structure of the related *Pyrococcus horikoshii* A-ATPase E subunit (Lokanath, N. K., Matsuura, Y., Kuroishi, C., Takahashi, N., and Kunishima, N. (2007) *J. Mol. Biol.* 366, 933–944). However, upon the addition of a peptide comprising the C-terminal 21 residues of the H subunit (or full-length H subunit), dimeric E subunit C-terminal domain dissociates to form a 1:1 heterodimer. NMR spectroscopy was used to show that H subunit C-terminal peptide binds to E subunit C-terminal domain via the terminal α-helices, with little involvement of the β-sheet region. Based on these data, we propose a structural model of the A-ATPase peripheral stalk.

The archaeal ATP synthase (A_1A_0-ATPase),[2] along with the related F_1F_0- and V_1V_0-ATPases (proton pumping vacuolar ATPases), is a rotary molecular motor (1–4). The rotary ATPases are bilobular in overall architecture, with one lobe comprising the water-soluble A_1, F_1, or V_1 and the other comprising the membrane-bound A_0, F_0, or V_0 domain, respectively. The subunit composition of the A-ATPase is $A_3B_3DE_2FH_2$ for the A_1 and CIK_x for the A_0. In the A_1 domain, the three A and B subunits come together in an alternating fashion to form a hexamer with a hydrophobic inner cavity into which part of the D subunit is inserted. Subunits D and F comprise the central stalk connection to A_0, whereas two heterodimeric EH complexes are thought to form the peripheral stalk attachment to A_0 seen in electron microscopy reconstructions (5, 6). In the A_0 domain (subunits CIK_x), the K subunits (proteolipids) form a ring that is linked to the central stalk by the C subunit, whereas the cytoplasmic N-terminal domain of the I subunit probably mediates the binding of the EH peripheral stalks to A_0, as suggested for the bacterial A/V-type enzyme (7). Although closer in structure to the proton-pumping V-ATPase, the A-ATPase functions *in vivo* as an ATP synthase, coupling ion motive force to ATP synthesis, most likely via a similar rotary mechanism as demonstrated for the bacterial A/V- and the vacuolar type enzymes (8, 9). During catalysis, substrate binding occurs sequentially on the three catalytic sites, which are formed predominantly by the A subunits. This is accompanied by conformation changes in the A_3B_3 hexamer that are linked to the rotation of the embedded D subunit together with the rotor subunits F, C, and the proteolipid ring. Each copy of K contains a lipid-exposed carboxyl residue (Asp or Glu), which is transiently interfaced with the membrane-bound domain of I during rotation, thereby catalyzing ion translocation. The EH peripheral stalks function to stabilize the A_3B_3 hexamer against the torque generated during rotation of the central stalk. Much work has been accomplished to elucidate the architectural features of the rotational and catalytic domains, especially in the related F- and V-type enzymes. However, the peripheral stalk complexes in the A- and V-type enzymes remain an area open to question. Although the stoichiometry of the peripheral stalks in the A/V-type and the vacuolar type ATPases have recently been resolved to two and three, respectively (6, 10), the overall structure of the peripheral stalk, including the nature of attachment to the A_3B_3 hexamer and I subunit (called subunit *a* in the F- and V-ATPase), is not well understood. Some structural information exists in the form of the A-ATPase E subunit C-terminal domain (11), although isolation from its binding partner H may have influenced its conformation.

Previously, our lab has characterized the *Thermoplasma acidophilum* A-ATPase E and H subunits individually and in complex (12). We found that despite their tendency to oligomerize when isolated separately, upon mixing, E and H form a tight heterodimer that was monodisperse and elongated in solution, which is consistent with its role as the peripheral stalk element in the A-ATPase. Here, we have expanded our study of the A-ATPase EH complex through the production of various N- and C-terminal truncation mutants of both binding partners. The data show that the EH complex is comprised of two distinct domains, one that contains both N termini interacting via a coiled-coil and a second that contains both C termini folded in a globular structure containing mixed secondary structure. Consistent with recent crystallographic data for the related A-ATPase from *Pyrococcus horiko-*

* This work was supported, in whole or in part, by National Institutes of Health Grants GM58600 and CA100246 (to S. W.).

[S] The on-line version of this article (available at http://www.jbc.org) contains supplemental Fig. S1–S4.

[1] To whom correspondence should be addressed. Tel.: 315-464-8703; Fax: 315-464-8750; E-mail: wilkenss@upstate.edu.

[2] The abbreviations used are: A_1, water-soluble domain of the A-ATPase; A_0, membrane-bound domain of the A-ATPase; MBP, maltose-binding protein; HSQC, heteroatom single quantum coherence.

shii (11), we found that the isolated C-terminal domain of the E subunit exists as a stable homodimer in solution. However, the addition of subunit H or a peptide consisting of the 21 C-terminal residues of the subunit to the dimeric C-terminal domain of subunit E resulted in dissociation of the homodimer with concomitant formation of a 1:1 heterodimer containing the C termini of both polypeptides. This study delineates and characterizes the two domains of the EH complex and will aid in the further exploration of the nature of peripheral stalk attachment and function in the intact A_1A_0-ATPase.

EXPERIMENTAL PROCEDURES

Protein Expression and Purification—All of the constructs used in this study were expressed as N-terminal fusions with *Escherichia coli* maltose-binding protein (MBP), which were isolated by amylose resin affinity chromatography and cleaved with protease. A summary of the constructs analyzed in this study is shown in Fig. 1*A*. Constructs $E_{NT1(2-99)}$, $E_{NT2(2-83)}$, $E_{CT1(83-185)}$, $E_{CT2(99-185)}$, $H_{NT(2-91)}$, and $H_{CT(91-111)}$ were subcloned, using conventional techniques, into the modified pMalc2e plasmid using 5′-KpnI and 3′-HindIII sites. The naturally occurring cysteine at position 121 in the E subunit was replaced by alanine as described (12). All of the resulting constructs were confirmed by DNA sequencing (Upstate Medical University DNA sequencing core facility). Plasmid DNA was expressed in Rosetta pLacI *E. coli* cells (Novagen), and fusion protein was purified and cleaved as previous (12). E_{NT1}, E_{NT2}, and E_{CT2} tend to aggregate when cleaved from MBP during purification, although E_{NT1} and E_{NT2} were found to be soluble when in complex with H or H_{NT} (see below). Separation of target proteins from cleaved MBP fusion was as follows: *E* and *H* were as described previously (12); H_{NT}-cleaved fractions were pooled, and most of the MBP was removed by a 60% ammonium sulfate precipitation and subsequent centrifugation at 13,000 × *g* for 30 min. Redissolved protein was further purified by gel filtration chromatography (Superdex 75; GE Healthcare; 16/50 column) in 25 mM sodium phosphate (pH 7), 0.5 mM EDTA, 0.02% sodium azide. E_{CT1}-cleaved fractions were pooled, concentrated to ~5 ml by ultrafiltration (5,000 molecular weight cut-off; VivaSpin) and dialyzed against 20 mM Tris-HCl (pH 8.0), 25 mM NaCl, 0.5 mM EDTA overnight. The sample was then passed over a 5-ml DEAE column (Sigma), which was then washed with 5CV of the dialysis buffer. MBP was captured by the column, and E_{CT1} was in the flow through and wash fractions. H_{CT}-cleaved fractions were pooled and boiled for 5 min, with subsequent centrifugation at 13,000 × *g* for 30 min. The supernatant was dialyzed against 25 mM Tris-HCl (pH 7.4), 10 mM NaCl, 0.5 mM EDTA (Buffer A). The sample was then passed over a 1-ml MonoQ column (GE Healthcare), washed with 10 CV Buffer A, and eluted with 0–80% of 20 mM Tris-HCl (pH 7.4), 0.5 mM EDTA, 500 mM NaCl in 20 CV (Buffer B). The samples analyzed by CD spectroscopy were prepared as follows: $E_{NT2}H_{NT}$-cleaved E_{NT2} and H_{NT} were mixed at a ~1:1.2 molar ratio. A majority of MBP and excess H_{NT} was removed by a 65% ammonium sulfate precipitation, followed by resuspension of the pellets in 25 mM Tris-HCl (pH 7.4), 10 mM NaCl, 0.5 mM EDTA and overnight dialysis against the same. Dialyzed sample was passed over a 1-ml MonoQ column (GE Healthcare), washed with 14 CV, and eluted in a step gradient (0–20% 2 CV; 20% 5 CV; 20–40% 15 CV). $E_{NT2}H_{NT}$ containing fractions were identified by SDS-PAGE, concentrated to ~1 ml by ultrafiltration (5,000 molecular weight cut-off; VivaSpin), and passed over a gel filtration column (Superdex 75; GE Healthcare; 16/50 column) equilibrated in 25 mM Tris-HCl (pH 7.4), 0.5 mM EDTA. $E_{CT1}H_{CT}$-cleaved E_{CT1} was pooled with a ~1:1.2 molar ratio of cleaved H_{CT}. The sample was then dialyzed against 20 mM Bis-Tris-HCl (pH 6.5), 25 mM NaCl, 0.5 mM EDTA and passed over a 5-ml DEAE column as described above. As in the E_{CT1} prep described above, $E_{CT1}H_{CT}$ flowed through the column; protein-containing fractions were concentrated and further purified by gel filtration as described above.

Size Exclusion Chromatography—The Superdex 75 HR 16/50 column, attached to an ÄKTA fast protein liquid chromatography (GE Healthcare) was calibrated with insulin (5.8 kDa), RNase A (15.2 kDa), green fluorescent protein (27 kDa), albumin (61.6 kDa), and blue dextran (~2×10^3 kDa).

CD Spectroscopy—Concentrated proteins were exchanged into 25 mM sodium phosphate (pH 7) and CD wavelength and temperature melt spectra were collected as previous (12). The protein concentrations of $E_{NT2}H_{NT}$, $E_{CT1}H_{CT}$, and EH were determined by absorbance at 277 nm of GdHCl denatured samples (13). A 0.2-cm cuvette was used for $E_{NT2}H_{NT}$ and $E_{CT1}H_{CT}$, whereas a 0.1-cm cuvette was used for EH. Secondary structure content was estimated by K2D2 (14, 15) and is summarized in supplemental Fig. S1.

Analysis of Complex Formation—The various E and H constructs were assayed for the ability to co-purify by ion exchange or co-elute by gel filtration in a manner equivalent to that of the full-length EH complex (12). The complexes characterized by CD ($E_{NT2}H_{NT}$ and $E_{CT1}H_{CT}$) were prepared as described above. When the target(s) were known not to remain in solution upon cleavage from MBP, the intact fusion was used to probe the interaction (full-length E and H can readily form a complex as MBP fusions; data not shown). Additionally, the technique taking advantage of the most resolved characteristic between the putative binding partners, predicted charge dispersion (ion exchange) or elution volume (gel filtration), was utilized. In the next section, "gel filtration" refers to the passage of 1 ml of ultrafiltered (5,000 molecular weight cut-off; VivaSpin) sample over a Superdex 75 HR 16/50 column attached to an ÄKTA fast protein liquid chromatography (GE Healthcare), which was equilibrated in either 25 mM sodium phosphate (pH 7), 0.5 mM EDTA, 0.02% azide, or 25 mM Tris-HCl (pH 7.4), 0.5 mM EDTA; "ion exchange" refers to sample dialysis against 25 mM Tris-HCl (pH 7.4), 10 mM NaCl, 0.5 mM EDTA, followed by ultraconcentration (5,000 molecular weight cut-off; Vivaspin) to 2 ml and passage over a 1-ml MonoQ column (GE Healthcare), which was washed with 10 CV of the dialysis buffer as Buffer A and eluted in 20 CV by a gradient of 0–80% 25 mM Tris-HCl (pH 7.4), 500 mM NaCl, 0.5 mM EDTA as Buffer B (buffers differ for E_{NT1} and *H* as noted). The resultant peak elution fractions from both techniques were analyzed by SDS-PAGE. The following complexes were analyzed for complex formation: E_{NT1} and *H*, MBP-E_{NT1} fusion was combined ~1:1.2 with purified H, followed by protease cleavage, a majority of MBP was removed by 60% ammonium sulfate precipitation, and the redissolved pellet was

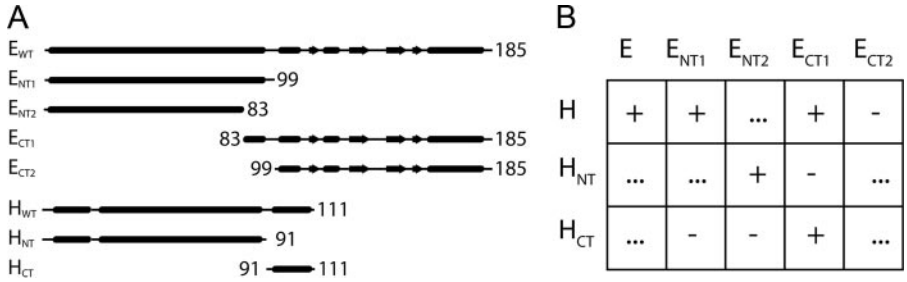

FIGURE 1. **Summary of the EH truncation mutants and their interaction.** *A*, schematic of full-length E and H subunits and truncation mutants used in this study. Secondary structure prediction was obtained from the PSIPRED prediction server. The *arrows*, *cylinders*, and *lines* denote predicted β-sheet, α-helix, and random coil content, respectively. *B*, table of interaction assay results. Positive and negative interactions are designated with (+ and −), indicating the ability/inability to co-purify by either ion exchange or gel filtration. Interactions not assessed in this study are marked (···).

dialyzed and analyzed by ion exchange, with 20 mM BisTris-HCl (pH 6.5), 25 mM NaCl, 0.5 mM EDTA as Buffer A, and 20 mM BisTris-HCl (pH 6.5), 500 mM NaCl, 0.5 mM EDTA as Buffer B; E_{NT1} and H_{CT}, MBP-E_{NT1} fusion was combined ~1:1.2 with purified H_{CT} and analyzed by ion exchange; E_{NT2} and H_{CT}, MBP-E_{NT2} fusion was combined ~1:1.2 with purified H_{CT} and analyzed by ion exchange; E_{CT1} and H, purified E_{CT1} was combined ~1:1.2 with purified H and analyzed by gel filtration; E_{CT1} and H_{NT}, MBP-H_{NT} fusion was combined ~1:1.2 with E_{CT1} and analyzed by ion exchange; and E_{CT2} and H, MBP-E_{CT2} fusion was combined ~1:1.2 with purified H and analyzed by gel filtration.

NMR Spectroscopy—Uniformly ^{15}N-labeled E_{CT1} and $E_{CT1}H_{CT}$ were produced in M9 medium with ^{15}N-NH_4Cl as the sole nitrogen source. ^{15}N and ^{13}C double-labeled samples were produced in a similar fashion, with the exception of 0.2% [^{13}C]glucose as the sole carbon source. [^{15}N]NH_4Cl and [$^{13}C_6$]glucose was from Isotec, Inc. The proteins were purified as described above and exchanged into 25 mM sodium phosphate, 0.5 mM EDTA, 0.02% azide, 7% D_2O. All of the spectra were recorded at 25 °C on a Bruker Avance 600-MHz spectrometer equipped with a HCN triple-axis gradient probe. Sequential assignment of the ^{15}N HSQC spectra was achieved with the HNCACB experiment supplemented with ^{15}N HSQC-nuclear Overhauser enhancement spectroscopy/total correlation spectroscopy experimental data. All of the NMR data were processed in Felix2004. Proton resonances were referenced by setting the 2,2-dimethyl-2-silapentane-5-sulfonate frequency as 0 ppm and extrapolating the ^{15}N and ^{13}C zero point frequencies as described (16). The secondary structure of $E_{CT1}H_{CT}$ was determined from α carbon and α proton chemical shift values using the chemical shift index protocol (17). Briefly, upfield or downfield changes in chemical shift from random coil values of greater than $\pm$0.1 ppm (for $^1H^\alpha$) and +0.8/−0.5 ppm (for $^{13}C^\alpha$) are scored as +1 or −1, respectively. The α-helix is assigned when four or more residues are −1 for $^1H^\alpha$ and/or +1 for $^{13}C^\alpha$. The β-strand is assigned when the inverse holds true for three or more residues.

Secondary Structure Prediction—For secondary structure and coiled-coil prediction, the PSIPRED (18) and parcoil2 (19) servers were used.

RESULTS AND DISCUSSION

Previously, we have shown that the *T. acidophilum* A-ATPase E and H subunits form a tight, monodisperse heterodimer with 1:1 stoichiometry (12). In the process of this study, it was found that the individual subunits tend to oligomerize and that formation of the EH heterodimer out-competes this tendency. Moreover, analytical ultracentrifugation and gel filtration experiments suggested an extended conformation for the EH complex, which is consistent with its role as the peripheral stalk element in the *T. acidophilum* A-ATPase. Here we expand on our study of the EH complex by dissecting out individual domains for analysis.

Domain Interactions in the EH Complex—To probe the regions of E and H that are required to form the EH heterodimer, N- and C-terminal truncation mutants were constructed and assayed for their ability to interact (Fig. 1). Putative binding partners were probed for their ability to either co-elute via gel filtration or co-purify via ion exchange in a manner consistent with that of the full-length EH complex (12). Fig. 1*B* summarizes the probed interactions and resulting observations. Overall, the binding studies revealed that the EH heterodimer is organized in two major domains: a coiled-coil domain comprised by the N termini of the two subunits and a C-terminal domain containing the globular C terminus of the E subunit bound to the C-terminal α-helix of H. Because the N- and C-terminal parts of the EH peripheral stalk complex appeared to represent stable entities on their own, the two domains were characterized independently as presented in the following sections.

Characterization of $E_{NT2}H_{NT}$ by CD Spectroscopy—The EH N-terminal coiled-coil domain was reconstituted by mixing individually expressed E_{NT2} (residues 2–83) and H_{NT} (residues 2–91), and the resulting $E_{NT2}H_{NT}$ complex was purified by ion exchange and size exclusion chromatography as described under "Experimental Procedures." Fig. 2*A* shows the elution profile of $E_{NT2}H_{NT}$ and intact EH. As can be seen, $E_{NT2}H_{NT}$ eluted with a lower apparent molecular mass than EH but still larger than its expected mass of ~22 kDa, suggesting that the N-terminal domain is also elongated as previously shown for intact EH (12). Fig. 2*B* shows SDS-PAGE of purified $E_{NT2}H_{NT}$ and full-length EH complex. To compare the secondary structure content of $E_{NT2}H_{NT}$ with that of the full-length complex, we carried out CD wavelength experiments (Fig. 2*C*). As can be seen, $E_{NT2}H_{NT}$ (*dotted line* in Fig. 2*C*) contains a greater per residue ellipticity than the full-length complex. Additionally, the ratio of the minima at 222 and 208 nm ($\theta_{222}/\theta_{208}$) is close to unity (0.99), an indication that $E_{NT2}H_{NT}$ contains a significant amount of coiled-coil secondary structure (20). A similar observation has been reported for the full-length EH complex (12) as well as the related EG heterodimer from yeast V-ATPase (21), indicating that the CD spectrum of the intact peripheral stalk complex is dominated by its N-terminal domain, which appears to comprises the majority, if not all, of the full-length EH complex coiled-coil content. This is consistent with an estimate of the secondary structure content for the two complexes based

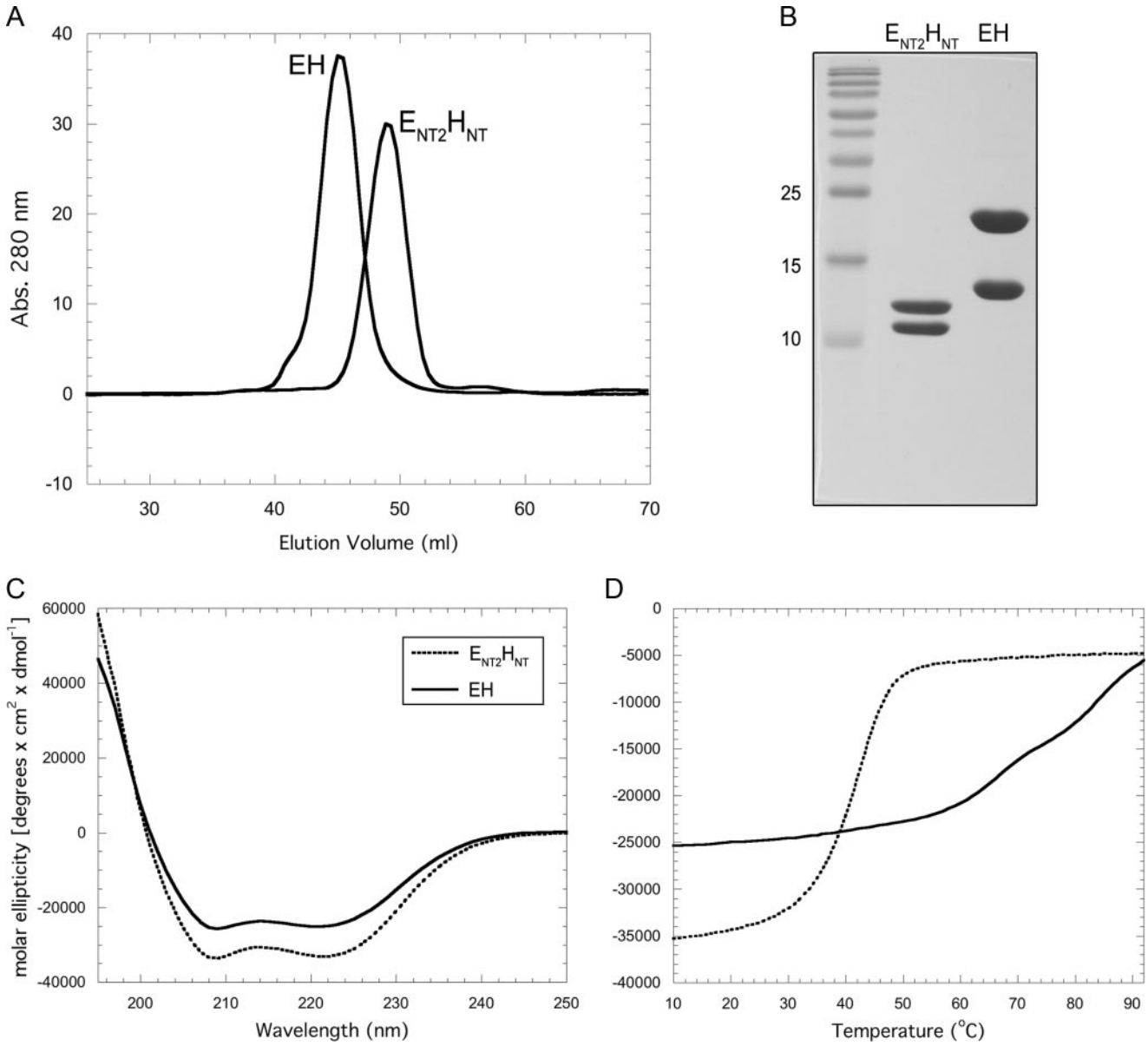

FIGURE 2. **Purification and characterization of $E_{NT2}H_{NT}$.** *A*, comparison of EH and $E_{NT2}H_{NT}$ gel filtration profiles. EH, which has been shown to be monodisperse and elongated in solution (12), elutes with an apparent molecular mass of ~52 kDa (35.5 kDa actual). $E_{NT2}H_{NT}$ elutes with a smaller apparent molecular mass of ~43 kDa (21.5 kDa actual), consistent with $E_{NT2}H_{NT}$, like intact EH, being elongated and monodisperse. *B*, 15% SDS-PAGE gel of $E_{NT2}H_{NT}$ and EH as visualized by Coomassie staining. Individual subunits were produced as fusion proteins and then reconstituted as described under "Experimental Procedures." *C*, CD wavelength scan of $E_{NT2}H_{NT}$ and EH in 10 mM sodium phosphate (pH 7) at 25 °C. Although both samples exhibit a union of the minima at 222 and 208 nm, indicating coiled-coil α-helical content, $E_{NT2}H_{NT}$ exhibits ~30% more molar ellipticity overall, suggesting that it represents the isolated coiled-coil domain. *D*, CD signal monitored at 222 nm as a function of increasing temperature (T_{melt}). EH, as previously reported, exhibits several cooperative transitions, whereas $E_{NT2}H_{NT}$ shows only a single strong transition, which may indicate it contains a single domain of EH, namely the coiled-coil domain. The reduced thermal stability may result from the isolation of the domain from the remainder of the complex.

on the CD data by K2D2 (14, 15), which indicated an α helical content of 76% *versus* 63% for $E_{NT2}H_{NT}$ and the intact EH complex, respectively (supplemental Fig. S1). The coiled-coil content of EH and $E_{NT2}H_{NT}$, as indicated by the CD measurements, is also consistent with the parcoil2 algorithm (19) that predicts coiled-coil formation with high probability for residues ~20–80 of subunit H and with somewhat lower certainty for residues 2–40 of subunit E. Interestingly, E_{NT2} and H_{NT} display more than 30% sequence identity (12), suggesting a similarity to other peripheral stalks that are known to have homodimeric coiled-coil domains (22). In particular, the handedness of the *E. coli b* subunit dimerization domain has been suggested to form either a left-handed (23) or right-handed coiled-coil (24) with varying degrees of offset. It has been speculated that the unusual arrangement of a right-handed coiled-coil with offset helices may function to counteract the torque generated during rotational catalysis in both the synthesis and hydrolysis direction (25). However, analysis of the primary sequences of the *T. acidophilum* A-ATPase E and H subunit N termini for the presence of the signature motifs characteristic for the two stranded left- or right-handed coiled-coil (heptad or hendecad repeats, respectively) is not conclusive, and it is therefore not known at this point which handedness the EH coiled-coil domain adopts (12).

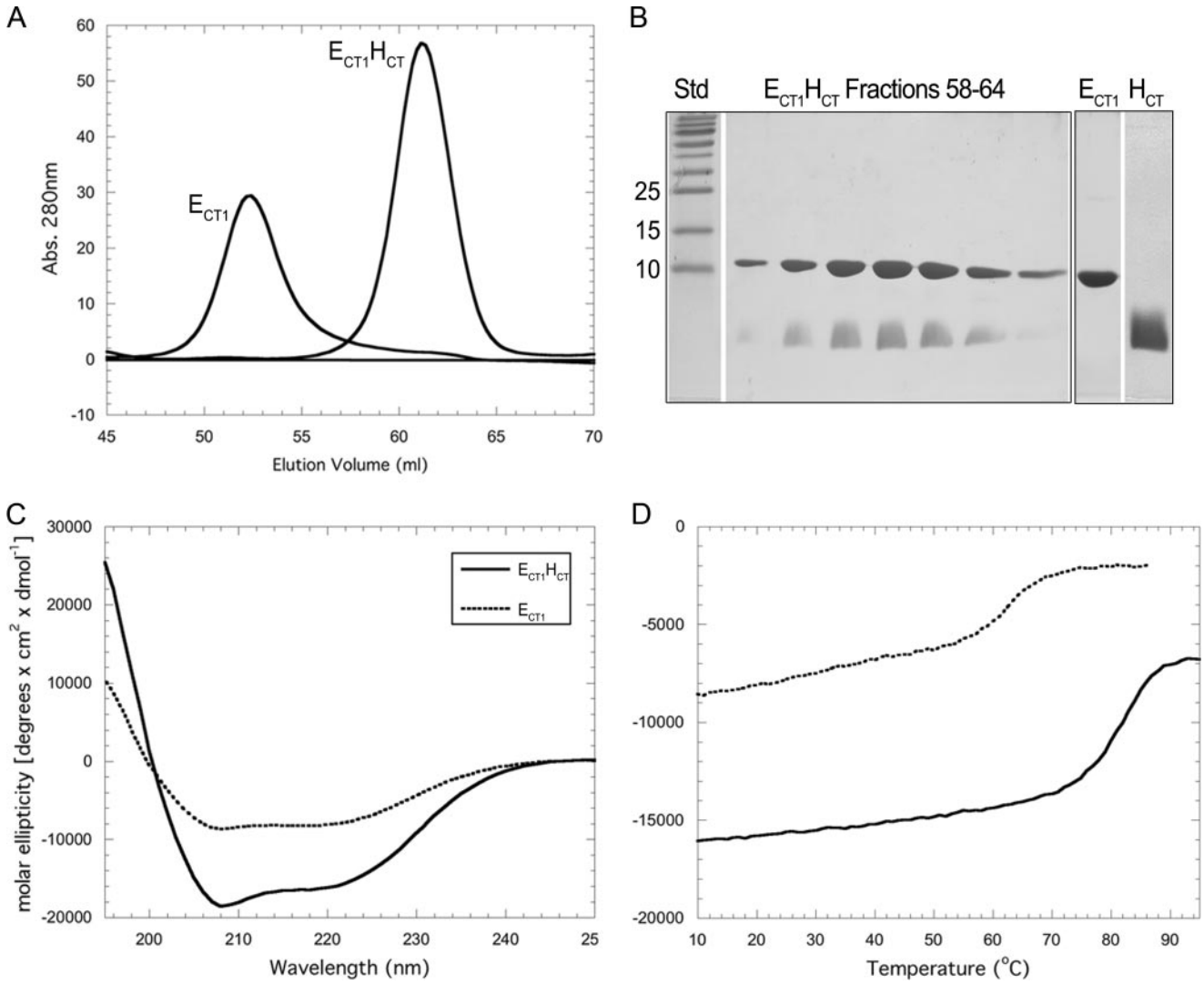

FIGURE 3. **Purification and characterization of E_{CT1} and $E_{CT1}H_{CT}$.** *A*, overlay of E_{CT1} and $E_{CT1}H_{CT}$ elution profiles collected during passage of the samples over a 16 × 500 mm Superdex 75 gel filtration column. Binding of H_{CT} to E_{CT1} resulted in an elution volume shift from 52 to 60.5 ml. This corresponds to a change in estimated molecular mass (spherical protein) from 35 to 22 kDa, compared with actual molecular masses of 12. kDa and 15 kDa for E_{CT1} and $E_{CT1}H_{CT}$, respectively. The change in elution volume suggests that H_{CT} binding effectively reduced the spherical volume of E_{CT1}, likely by out-competing homodimer formation. *B*, 15% SDS-PAGE gel of the $E_{CT1}H_{CT}$ elution peak and individually purified components visualized by Coomassie staining. E_{CT1} and H_{CT} were produced individually as fusion proteins and reconstituted as described under "Experimental Procedures." *C*, CD wavelength scan of E_{CT1} and $E_{CT1}H_{CT}$ in 10 mM sodium phosphate (pH 7) at 25 °C. Although retaining a shape indicative of mixed secondary structure, $E_{CT1}H_{CT}$ exhibits a greater molar ellipticity than E_{CT1}. Although this may be partially explained by the additional α-helical content contributed by H_{CT}, it is also likely that H_{CT} stabilizes E_{CT1} fold. This is further supported by the increase in thermal stability observed for $E_{CT1}H_{CT}$ *versus* E_{CT1} alone (*D*) and additionally studied in Fig. 4.

Additionally, we probed the thermal stability of $E_{NT2}H_{NT}$ by observing the CD signal at 222 nm as a function of temperature. The resultant graph shown in Fig. 2*D* (*dotted line*) reveals a single, strongly cooperative transition at ~40 °C, which is unlike the several weaker transitions observed for the full-length complex (*solid line* in Fig. 2*D*). The presence of a single transition suggests that $E_{NT2}H_{NT}$ is composed of a single cooperative element, which, from the above CD wavelength scan data, is probably represented by the coiled-coil domain. The reduced temperature of this transition, compared with any observed for intact EH, may result from the isolation of the domain from the remainder of the complex.

The unequal length of E_{NT2} (83 residues) and H_{NT} (91 residues) suggests that H_{NT} has an ~10-residue overhang on either the N- or C-terminal end of E_{NT2}. To determine which end of H_{NT} represents the overhang, we subjected $E_{NT2}H_{NT}$ and full-length EH complex to limited proteolysis by trypsin followed by mass spectrometry (supplemental Fig. S2). The data indicate that trypsin is able to quickly cleave the N terminus of H after the arginine at position 5, resulting in a comparably stable EH″ or $E_{NT2}H_{NT}$″ complex with an intact H or H_{NT} C terminus. Because there are two trypsin cleavage sites in the C-terminal 10 residues of H_{NT}, we conclude that the H_{NT} overhang occurs at the N-terminal end of subunit H.

Characterization of E_{CT1} and Interaction of E_{CT1} with H_{CT}— Guided by two-hybrid interaction studies in the related V-ATPase from yeast (26)[3] and in an effort to generate suitable domains of the peripheral stalk subunits for structural studies, we initially generated a series of E subunit truncations including

[3] P. M. Kane, personal communication.

the E_{CT1} construct comprised of residues 83–185 (Fig. 1*A*). E_{CT1} was expressed in *E. coli* as an MBP fusion and purified via affinity and size exclusion chromatography as described under "Experimental Procedures." Fig. 3*A* shows the size exclusion chromatography profile of the purified E_{CT1} domain. As can be seen, isolated E_{CT1} elutes at a volume corresponding to an apparent molecular mass of 35 kDa (~52 ml), suggesting that E_{CT1} behaves as a dimer in solution. This observation is consistent with a recent crystal structure of the C-terminal domain (residues 81–198) of the E subunit of the related A-ATPase from *P. horikoshii* that showed two subunit E C-terminal domains interacting via their N- and C-terminal α-helices to form a dimer (11). However, as we have previously reported, no E subunit dimerization is seen in the full-length EH complex, suggesting that dimer formation in the subunit E C-terminal domain is a result of the absence of its binding partner, subunit H. We therefore initially tested whether E_{CT1} dimer was able to interact with full-length subunit H by performing gel filtration and NMR titration experiments. Both approaches showed a dramatic change in the behavior of E_{CT1}, indicating a high affinity interaction between the two proteins (for NMR titration, see supplemental Fig. S3). No interaction was observed between E_{CT1} and H_{NT}, indicating that the interaction between E_{CT1} and full-length subunit H was mediated by the C-terminal 21 residues of subunit H (Fig. 1). We therefore expressed the C-terminal 21 residues of subunit H (H_{CT}) as N-terminal fusion with MBP and purified the peptide after removal of MBP as described under "Experimental Procedures." Fig. 3*A* shows the gel filtration profile of E_{CT1} upon binding of H_{CT}. As can be seen, a shift in peak elution from 52 ml for free E_{CT1} to 60.5 ml for $E_{CT1}H_{CT}$ complex is observed, corresponding to a change in apparent molecular mass from 35 kDa (for E_{CT1}) to 22 kDa (for $E_{CT1}H_{CT}$), which is close to the

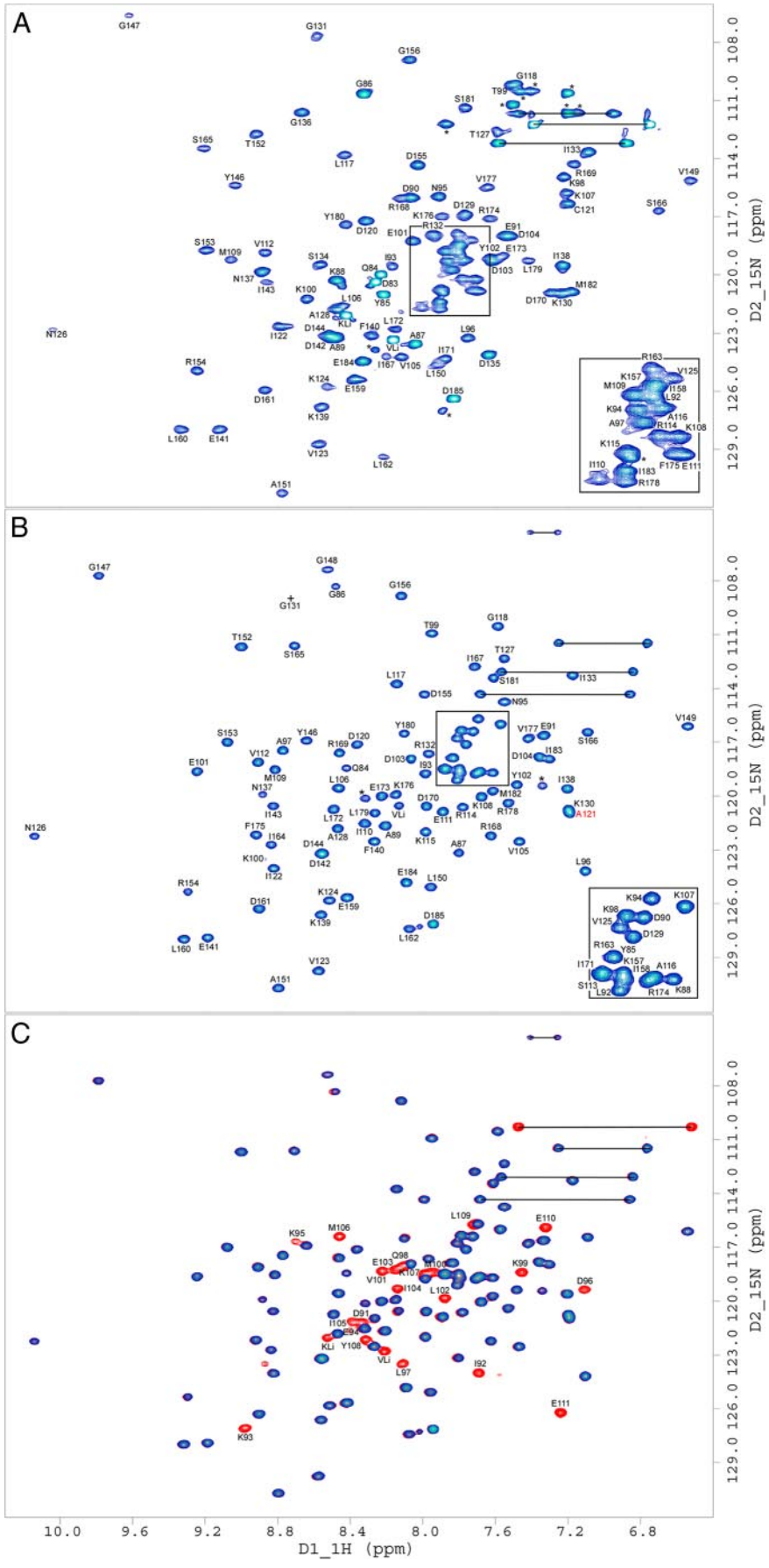

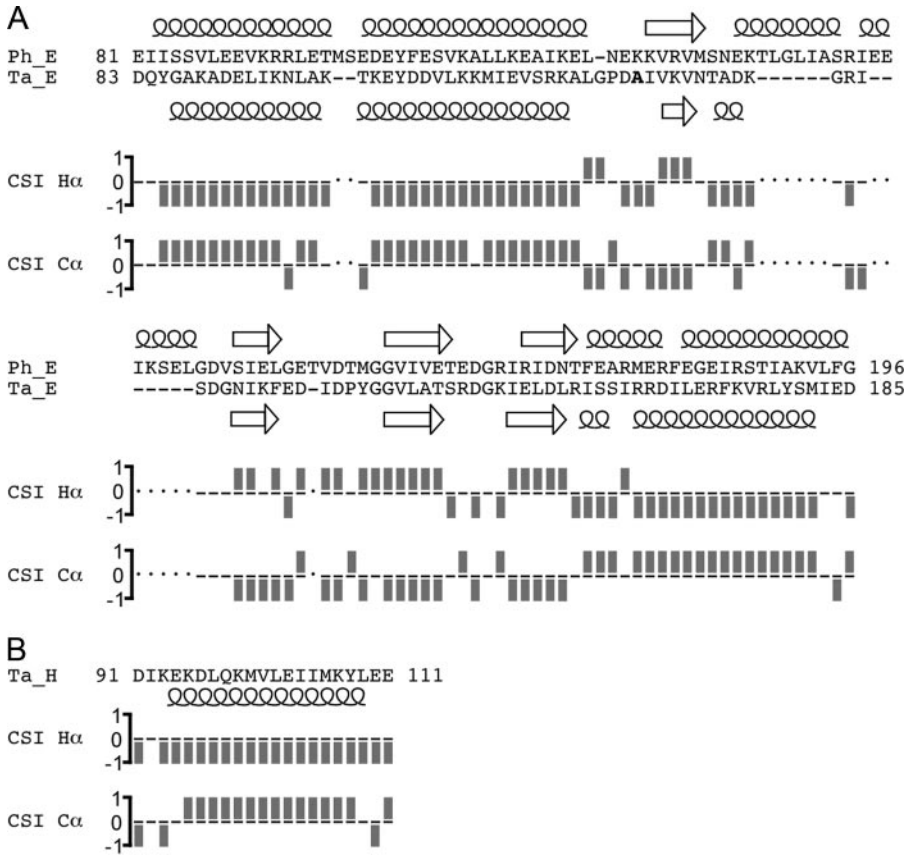

FIGURE 5. **Secondary structure analysis of $E_{CT1}H_{CT}$ as carried out by the chemical shift index protocol.** *A*, the sequence alignment of the *T. acidophilum* E_{CT1} (Ta_E_{CT1}) and the *P. horikoshii* E_{CT} (Ph_E_{CT}) was performed manually and refined by secondary structure comparison. Note that Ph_E_{CT} has two α-helices connecting β-strands 1 and 2 that are significantly shorter in Ta_E_{CT1}. The secondary structure for Ph_E_{CT} (from the crystal structure; Ref. 11) and Ta_E_{CT1} (from the H^{α} and C^{α} chemical shift values using the chemical shift index (*CSI*) protocol as described under "Experimental Procedures"). The overall high degree of secondary structure similarity between the two proteins suggests that Ph_E_{CT} is a good model for Ta_E_{CT1}. Furthermore, the retention of secondary structure in Ta_E_{CT1} when bound to H_{CT}, as shown here, indicates that the break up of Ta_E_{CT1} dimers by the addition of H_{CT} (Figs. 3 and 4) is accompanied by a rearrangement of secondary structure elements rather than a change in composition of the same. *B*, the secondary structure analysis of H_{CT} indicates α-helix for residues ~95–108. See supplemental Fig. S4 for absolute deviations of $^{1}H\alpha$ and $^{13}C\alpha$ chemical shift values from random coil values.

predicted molecular mass of 15 kDa for the heterodimer (Fig. 3*B*). The change in apparent molecular weight indicates that binding of H_{CT} occurs with sufficient affinity to disrupt the E_{CT1}-E_{CT1} homodimer interface upon heterodimer formation.

Characterization of $E_{CT1}H_{CT}$ by CD Spectroscopy and Comparison with E_{CT1}—To assess the conformational changes occurring in E_{CT1} upon the binding of H_{CT}, we performed CD wavelength and temperature melt experiments. The CD spectrum of $E_{CT1}H_{CT}$ shows a greater molar ellipticity compared with the spectrum of isolated E_{CT1} domain (Fig. 3*C*). Specifically, as expected from the prediction of H_{CT} as helical, the minima at 208 nm is more pronounced for $E_{CT1}H_{CT}$ than E_{CT1}. However, it is unlikely that this contribution alone provides a complete explanation for the increase in the magnitude of the signal intensity. Instead, the binding of H_{CT} likely stabilizes a particular conformation of E_{CT1}. This is further supported by the respective thermal stabilities of E_{CT1} *versus* $E_{CT1}H_{CT}$ as observed by monitoring the CD signal at 222 nm as a function of temperature (Fig. 3*D*). Both E_{CT1} and $E_{CT1}H_{CT}$ exhibit single, cooperative transitions, although the transition for $E_{CT1}H_{CT}$ is both at a higher temperature and more pronounced (82 °C for $E_{CT1}H_{CT}$ compared with 63 °C for E_{CT1}). These observations imply that $E_{CT1}H_{CT}$ is more stable than isolated, homodimeric E_{CT1}.

NMR Spectroscopy of E_{CT1} and $E_{CT1}H_{CT}$—To further explore the binding of E_{CT1} to H_{CT}, we analyzed and compared ^{15}N HSQC spectra of ^{15}N-labeled E_{CT1} alone and in complex with labeled and unlabeled H_{CT} (Fig. 4). Fig. 4*A* shows a $^{1}H/^{15}N$ HSQC experiment for the uniformly ^{15}N-labeled E_{CT1} domain. As can be seen, the spectrum shows generally good chemical shift dispersion of the backbone amide resonances, typical for a protein with mixed secondary structure. Yet some of the peaks appear broadened and of unequal intensity, indicative of dimer/oligomer formation at the concentrations used for NMR spectroscopy. However, a dramatic change in the appearance of the E_{CT1} spectrum is observed upon the addition of full-length H or H_{CT} peptide. A titration of ^{15}N-labeled E_{CT1} with unlabeled H leads to the appearance of additional resonances at substoichiometric ratios, indicative of high affinity binding of H to E_{CT1} (supplemental Fig. S3). Fig. 4*B* shows a $^{1}H/^{15}N$ HSQC spectrum of purified $E_{CT1}H_{CT}$ complex (^{15}N-E_{CT}, ^{14}N-H_{CT}), which is more resolved and homogenous in regards to peak intensity when compared with that of E_{CT1} alone (Fig. 4*A*). This effect is global and suggests a gain in structural stability of E_{CT1} in response to the binding of H_{CT}. This is consistent with a reduction in overall volume and, again, supports the breakup of E_{CT1} dimers by the addition of H_{CT}. In Fig.

FIGURE 4. **^{15}N HSQC NMR spectra of E_{CT1} and $E_{CT1}H_{CT}$.** Two-dimensional $^{1}H/^{15}N$ HSQC NMR spectra taken at 298 K in 25 mM sodium phosphate (pH 7), 0.5 mM EDTA, and 0.02% NaN_3. Spectra presented are: E_{CT1} (*A*), $E_{CT1}H_{CT}$ where H_{CT} is unlabeled for clarity (*B*), and where $E_{CT1}H_{CT}$ is fully labeled (*red*) and is overlaid by the partially labeled spectrum from *B* in *blue* (*C*). The observed change in E_{CT1} behavior upon H_{CT} binding, explored in Fig. 3, is further evidenced here by the global improvement in backbone amide peak signal dispersion and homogeneity indicative of E_{CT1} fold stabilization by H_{CT} binding. Side chain amide peaks are linked by *black horizontal lines*. Resonances marked with an *asterisk* belong to amino acid side chains (*e.g.* Arg) or residues that could not be assigned because of overlap/poor signal to noise. KLi and VLi are part of the N-terminal linker (GPKVP). For E_{CT1} and $E_{CT1}H_{CT}$, Ser^{113}, Gly^{148}, Ile^{164}, Ser^{134}, Asp^{135}, and Gly^{136} could not be assigned, respectively. The mutation Ta_E C121A has been described previously (Ref. 12; indicated by the *red label* in *B*). The concentration of NMR samples was between 0.5 and 1 mM.

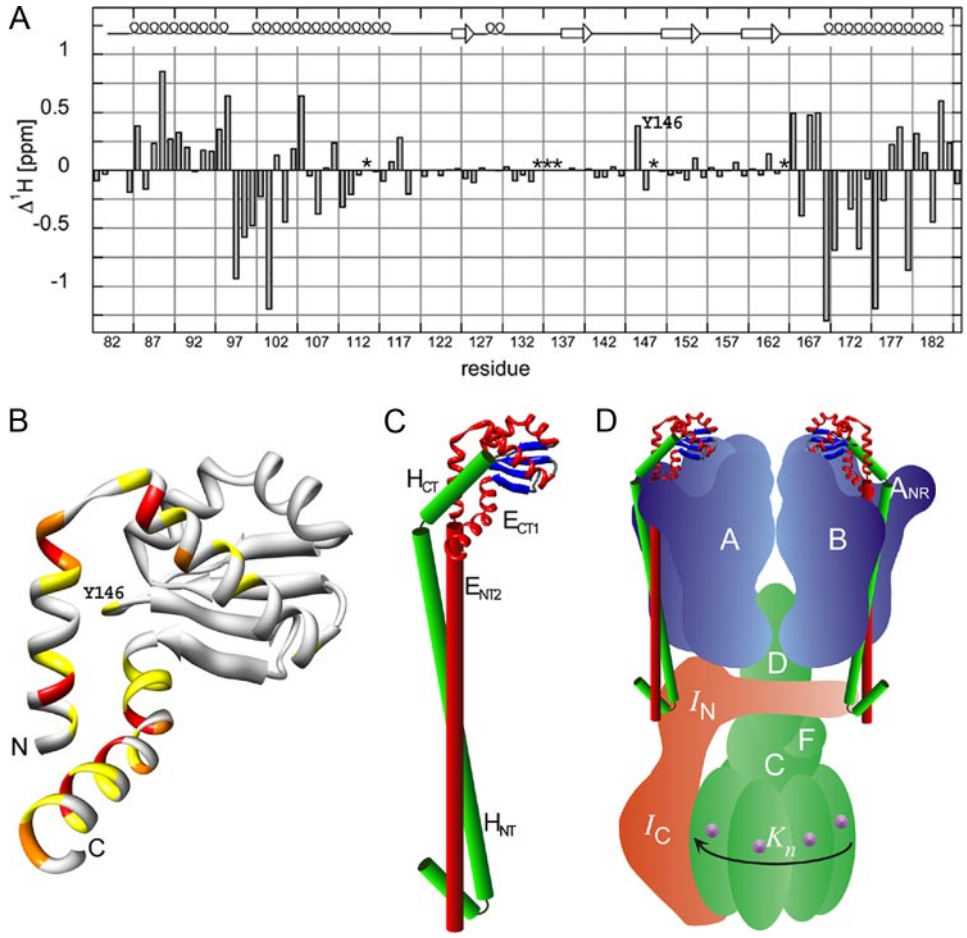

FIGURE 6. **Analysis of E_{CT1} chemical shift change upon the addition of H_{CT} and a model of the proposed domain arrangement in the full-length EH peripheral stalk complex.** Assignment of the ^{15}N HSQC spectra presented in Fig. 4 permitted the calculation of E_{CT1} amide-proton chemical shift changes ($\Delta^1H\delta$) upon binding H_{CT}. *A*, as can be seen, the majority of residues experiencing the most significant chemical shift perturbation upon H_{CT} binding are located in the N- and C-terminal helices of E_{CT1} (residues for which no assignments could be obtained in either the E_{CT1} (Ser[113], Gly[148], and Ile[164]) or $E_{CT1}H_{CT}$ (Ser[134], Asp[135], and Gly[136]) spectra are marked with an *asterisk*). *B*, the positions analogous to the Ta_E_{CT1} residues undergoing the largest chemical shift changes are highlighted in the available crystal structure of Ph_E_{CT} with one dimer partner removed (Protein Data Bank code 2dma; Ref. 11). The largest change in chemical shift in the middle portion of the structure is experienced by Tyr[146], which can be seen located close to the N- and C-terminal α-helices of Ph_E_{CT} in the crystal structure (Ta_E Y146 corresponds to Ph_E M157). *C*, H_{CT}, modeled as an α-helix and guided by the data presented here, is docked onto the Ph_E_{CT} crystal structure monomer. Continuing below the globular $E_{CT1}H_{CT}$ domain, the N-terminal domain, $E_{NT2}H_{NT}$, is modeled as a pair of parallel helices, representing the coiled-coil domain. We speculate that the N-terminal α-helix of H_{NT} is folded back to interact with and stabilize the N-terminal ends of the coiled-coil domain. *D*, the resulting EH model placed into a schematic model of the *T. acidophilum* A-ATPase. The stoichiometry of the EH peripheral stalks has recently been determined for the related A/V-ATPase from *T. thermophilus* (6).

4*C* we assessed the status of H_{CT} when bound to E_{CT1} by superimposing the spectrum of fully ^{15}N- labeled $E_{CT1}H_{CT}$ (*red*) with the spectrum of $E_{CT1}H_{CT}$ where E_{CT1} alone was ^{15}N labeled (*blue*). The overall chemical shift dispersion of the H_{CT} resonances indicates a stable conformation of H_{CT} when bound to E_{CT1}. For both isolated E_{CT1} (Fig. 4*A*) and $E_{CT1}H_{CT}$ complex (Fig. 4, *B* and *C*), amide resonances were sufficiently resolved to allow for the unambiguous assignment of the majority of peaks, which are notated in the respective spectra.

Secondary Structure Analysis of $E_{CT1}H_{CT}$—In the available *P. horikoshii* E subunit C terminus (Ph_E_{CT}) crystal structure, dimerization is mediated by a domain swap, whereby the N-terminal α-helix of one monomer interacts with the C-terminal α-helix of the other monomer and vice versa (11). To assess whether Ph_E_{CT} is an appropriate model for *T. acidophilum* E subunit C-terminal domain (Ta_E_{CT1}) bound to Ta_H_{CT}, we analyzed the secondary structure of Ta_E_{CT1} and compared it with the crystal structure of Ph_E_{CT}. Fig. 5 summarizes the secondary structure content of the *P. horikoshii* E_{CT} dimer and the *T. acidophilum* $E_{CT1}H_{CT}$ complex. The secondary structure assignment of Ta_$E_{CT1}H_{CT}$ is based on C^α proton and carbon chemical shift analysis by the chemical shift index protocol (Ref. 17 and supplemental Fig. S4 for the differences of $^1H^\alpha$ and $^{13}C^\alpha$ chemical shifts from random coil values). As can be seen, the secondary structure content of the C-terminal domains of the two related E subunits is very similar, indicating that Ph_E_{CT} is an appropriate model structure for Ta_E_{CT1} bound to H_{CT}. The similar secondary structure content further suggests that binding of Ta_H_{CT} to Ta_E_{CT1} does not alter the overall secondary structure but rather results in repacking of the N- and C-terminal α-helices of E subunit C-terminal domain to accommodate the C-terminal α-helix of subunit H. The data also show that residues ~95–108 of subunit H are folded as an α-helix, and it seems likely that this α-helix together with the N- and C-terminal α-helices of E_{CT1} form a three α-helix bundle.

Amide-Proton Chemical Shift Changes ($\Delta^1H\delta$) of E_{CT1} upon Binding of H_{CT}—Our observation of $E_{CT1}H_{CT}$ complex formation and the lack of H_{CT} binding to E_{CT2} suggests that H_{CT} disrupts E_{CT1} dimerization by interacting with its N-terminal α-helix. However, E_{NT1}, which contains this helix on its C terminus, cannot form a similarly tight complex with H_{CT} (Fig. 1*B*). Additionally, Fig. 5 demonstrates that H_{CT} binding to E_{CT1} does not confer major changes in secondary structure content but rather a reordering of terminal helices. To probe this further we assessed the backbone amide-proton chemical shift change of E_{CT1} residues upon binding of H_{CT} (Fig. 6*A*). E_{CT1} residues undergoing an amide ^1H chemical shift change upon H_{CT} binding of greater than 0.75, 0.5, and 0.25 ppm are highlighted in the crystal structure of Ph_E_{CT} in *red*, *orange*, and *yellow*, respectively. As can be seen in Fig. 6*B*, the residues experiencing the greatest chemical shift perturbation lie in the N- and C-terminal α-helices of E_{CT1}, indicating that

both N- and C-terminal α-helices of E_{CT1} are involved in binding H_{CT}.

Structural Model of Intact EH Complex—In the full-length EH complex, the N-terminal ends of both E_{CT1} and H_{CT} are joined with their N-terminal domains, which, as shown in Fig. 2, appear to be folded as a coiled-coil for most of their length. Fig. 6*C* shows our current working model of the domain architecture of the A-ATPase peripheral stalk, which is based on the crystal structure of *P. horikoshii* A-ATPase E subunit C-terminal domain and the results presented here. Additional experimental support for the interaction of the N termini of E and H subunits has recently been obtained from peptide binding studies, which indicated an interaction between residues H^{1-47} and E^{41-60} for the related A-ATPase from *Methanocaldococcus janaschii* (27). Secondary structure prediction (Fig. 1 and Ref. 12) predicts that residues 5–19 at the N terminus of subunit H are folded as an α-helix followed by a turn (residues 20–22). Based on this prediction and the proteolysis experiment mentioned above, we speculate that the N-terminal α-helix of subunit H is folded back to interact with, and stabilize, the two N-terminal ends of the coiled-coil domain. The resulting EH heterodimer model is ~150 Å long, consistent with its role as peripheral stalk. The arrangement of the EH peripheral stalk in the schematic model of the A-ATPase is shown in Fig. 6*D*. As mentioned above, two EH (EG) peripheral stalks have been found in the related bacterial A/V-type ATPase from *Thermus thermophilus* (6). We speculate that both peripheral stalks interact via their N-terminal domains with the elongated N-terminal domain of the I subunit, whereas their C-terminal domains are bound to the N-terminal regions of two of the three B subunits. Such an arrangement would be consistent with chemical cross-linking data that place the related EG heterodimer of the vacuolar ATPase along the surface of the B subunit (28). These results together with cross-linking experiments conducted with the A-ATPase from *Methanosarcina mazei* Gö1, which place the C-terminal region of the H subunit near the N-terminal region of one of the A subunits (29), suggest that the binding region for the EH (or EG) heterodimer is near a subunit AB interface as shown in Fig. 6*D*. Interestingly, three (subunit EG) peripheral stalks have been found in the related eukaryotic V-ATPase (10), and based on our recent three-dimensional reconstruction of the same enzyme (30), we have proposed that the third EG peripheral stalk is anchored to the membrane-bound *a* subunit via the V-ATPase C subunit (Vma5p), a subunit not found in the A- or A/V-type enzyme.

Concluding Remarks—It has been suggested that the progenitor rotary ATPase most likely resembled the bacterial F_1F_0-ATPase (31) and that the A-type, followed by the V-type, arose sometime later. This is supported by the so-called tree of life, which indicates a branching off of bacteria, before archaea, on the way to the eukaryotic "limb" (32). The gross morphological similarities of the F-, A-, and V-type motors and the nature of the A-type as being a "chimera" of F- and V-type attributes have been noted (33). Specifically, the peripheral stalks, although differing in subunit composition and complexity, carry out a similar role of stabilizing the hexamer against the torque generated during central stalk rotation. In the simplest case, the F-type peripheral stalk is composed of two copies of the *b* subunit and a single copy of the δ subunit (nomenclature of the bacterial enzyme). The N-terminal transmembrane α-helices of the *b* dimer anchor the stalk to subunit *a* of the F_0 sector, whereas the C terminus of one of the *b* subunits (b_{CT}) connects to the C terminus of δ (δ_{CT}). It is the N terminus of δ, which provides the connection to the hexamer via the N-terminal α-helix of one of the α subunits (34). Interestingly, there is evidence to support a fusion event between the respective C termini of δ and *b* to form the A/V-type peripheral stalk subunit E as well as the related FliH subunit of the T3SS secretion system. Namely, there is significant sequence similarity to *b* in the N termini of subunits E and FliH, in addition to similarity to δ_{CT} in their C termini (35, 36). Additionally, we have detected ~30% identity between E_{NT2} and H_{NT} (12), which may be a vestige of the *b* homodimer, and G (H of the A-ATPase is G in the V-ATPase) has been reported to have weak identity to bacterial *b* (37). However, the lack of a counterpart for the N terminus of δ and the presence of multiple stalks in the A/V-type enzymes imply that the connection to the hexamer may be unlike that observed in the F-type enzyme (34).

Our work here further resolves the A-ATPase EH peripheral stalk complex through the identification and characterization of the $E_{NT2}H_{NT}$ coiled-coil domain and the $E_{CT1}H_{CT}$ globular domain. In the coiled-coil $E_{NT2}H_{NT}$ domain, the subunits are parallel in orientation with H_{NT} being shifted down about 10 residues with respect to the N terminus of E_{NT2}. This domain is likely analogous to the coiled-coil region of the bacterial F-type *b* dimer and may provide a unique opportunity to study the possible function of the peripheral stalk coiled-coil domain in the transient storage of energy during catalysis (38). The $E_{CT1}H_{CT}$ complex is of particular interest in the light of our observations, which suggest a significant repacking of the terminal helices of E_{CT1} in response to binding H_{CT}. $E_{CT1}H_{CT}$, as opposed to the dimer form of E_{CT1}, likely represents the physiologically relevant form of the EH complex C terminus and will provide a valuable system in which to study the possibly unique interaction of an A/V-type peripheral stalk with the A_3B_3 hexamer.

Acknowledgments—We thank Dave Kiemle from the SUNY-ESF Analytical Instrumentation Facility for assistance with the NMR spectroscopy experiments, Lee Parsons for help with the mass spectrometry analysis, and Dr. Stewart Loh for help with the CD spectroscopy.

REFERENCES

1. Müller, V., and Grüber, G. (2003) *Cell. Mol. Life. Sci.* **60,** 474–494
2. Forgac, M. (2007) *Nat. Rev. Mol. Cell Biol.* **8,** 917–929
3. Boyer, P. D. (1997) *Annu. Rev. Biochem.* **66,** 717–749
4. Wilkens, S. (2005) *Adv. Prot. Chem.* **71,** 345–382
5. Coskun, U., Chaban, Y. L., Lingl, A., Müller, V., Keegstra, W., Boekema, E. J., and Grüber, G. (2004) *J. Biol. Chem.* **279,** 38644–38648
6. Esteban, O., Bernal, R. A., Donohoe, M., Videlar, H., Sharon, M., Robinson, C. V., and Stock, D. (2007) *J. Biol. Chem.* **283,** 2595–2603
7. Yamamoto, M., Unzai, S., Saijo, S., Ito, K., Mizutani, K., Suno-Ikeda, C., Yabuki-Miyata, Y., Terada, T., Toyama, M., Shirouzu, M., Kobayashi, T., Kakinuma, Y., Yamato, I., Yokoyama, S., Iwata, S., and Murata, T. (2008) *J. Biol. Chem.* **283,** 19422–19431
8. Imamura, H., Nakano, M., Noji, H., Muneyuki, E., Ohkuma, S., Yoshida, M., and Yokoyama, K. (2003) *Proc. Natl. Acad. Sci. U. S. A.* **100,**

2313–2315
9. Hirata, T., Iwamotot-Kihara, A., Sun-Wada, G.-H., Okajima, T., Wada, Y., and Futai, M. (2003) *J. Biol. Chem.* **277,** 23714–23719
10. Kitagawa, N., Mazon, H., Heck, A. J., and Wilkens, S. (2008) *J. Biol. Chem.* **283,** 3329–3337
11. Lokanath, N. K., Matsuura, Y., Kuroishi, C., Takahashi, N., and Kunishima, N. (2007) *J. Mol. Biol.* **366,** 933–944
12. Kish-Trier, E., Briere, L. K., Dunn, S. D., and Wilkens, S. (2008) *J. Mol. Biol.* **375,** 673–685
13. Gill, S. C., and von Hippel, P. H. (1989) *Anal. Biochem.* **182,** 319–326
14. Andrade, M. A., Chacon, P., Merelo, J. J., and Moran, F. (1993) *Protein Eng.* **6,** 383–390
15. Perez-Iratxeta, C., and Andrade-Navarro, M. A. (2007) *BMC Struct. Biol.* **8,** 25
16. Wishart, D. S., Bigam, C. G., Yao, J., Abildgaard, F., Dyson, H. J., Oldfield, E., Markley, J. L., and Sykes, B. D. (1995) *J. Biomol. NMR* **6,** 135–140
17. Wishart, D. S., and Sykes, B. D. (1994) *Methods Enzymol.* **239,** 363–392
18. Jones, D. T. (1999) *J. Mol. Biol.* **292,** 195–202
19. McDonnell, A. V., Jiang, T., Keating, A. E., and Berger, B. (2006) *Bioinformatics* **22,** 356–358
20. Lau, S. Y., Taneja, A. K., and Hodges, R. S. (1984) *J. Biol. Chem.* **259,** 13253–13261
21. Féthière, J., Venzke, D., Diepholz, M., Seybert, A., Geerlof, A., Gentzel, M., Wilm, M., and Böttcher, B. (2004) *J. Biol. Chem.* **279,** 40670–40676
22. Dunn, S. D., Revington, M., Cipriano, D. J., and Shilton, B. H. (2000) *J. Bioenerg. Biomembr.* **32,** 347–355
23. Wise, J. G., and Vogel, P. D. (2008) *Biophys. J.* **94,** 5040–5045
24. Wood, K. S., and Dunn, S. D. (2007) *J. Biol. Chem.* **282,** 31920–31927
25. Del Rizzo, P., Bi, Y., and Dunn, S. D. (2006) *J. Mol. Biol.* **364,** 735–746
26. Ohira, M., Smardon, A. M., Charsky, C. M., Liu, J., Tarsio, M., and Kane, P. M. (2006) *J. Biol. Chem.* **281,** 22752–22760
27. Gayen, S., Balakrishna, A. M., Biukovic, G., Yulei, W., Hunke, C., and Grüber, G. (2008) *FEBS J.* **275,** 1803–1812
28. Arata, Y., Baleja, J. D., and Forgac, M. (2002) *J. Biol. Chem.* **277,** 3357–3363
29. Schäfer, I., Rössle, M., Biukovic, G., Müller, V., and Grüber, G. (2006) *J. Bioenerg. Biomembr.* **38,** 83–92
30. Zhang, Z., Zheng, Y., Mazon, H., Milgrom, E., Kitagawa, N., Kish-Trier, E., Heck, A. J. R., Kane, P. M., and Wilkens, S. (2008) *J. Biol. Chem.* **283,** 35983–35995
31. Cross, R. L., and Müller, V. (2004) *FEBS Lett.* **576,** 1–4
32. Woese, C. R. (2000) *Proc. Natl. Acad. Sci. U. S. A.* **97,** 8392–8396
33. Schäfer, G., and Meyering-Vos, M. (1992) *Biochim. Biophys. Acta* **1101,** 232–235
34. Wilkens, S., Borchardt, D., Weber, J., and Senior, A. E. (2005) *Biochemistry* **44,** 11786–11794
35. Lane, M. C., O'Toole, P. W., and Moore, S. A. (2006) *J. Biol. Chem.* **281,** 508–517
36. Pallen, M. J., Bailey, C. M., and Bearson, S. A. (2006) *Protein Sci.* **15,** 935–941
37. Supeková, L., Supek, F., and Nelson, N. (1995) *J. Biol. Chem.* **270,** 13726–13732
38. Neukirch, S., Goriely, A., and Hausrath, A. C. (2008) *Phys. Rev. Lett.* **100,** 038105